

Phase diagram of the $\text{TlGaS}_2\text{-CdS}$ system and optical properties of a $\text{TlGaS}_2\text{:Cd}^{2+}$ crystal

Lyudmyla PISKACH^{1*}, Galyna MYRONCHUK², Ganna MAKHNOVETS²

¹ *Department of Inorganic and Physical Chemistry, Lesya Ukrainka Eastern European National University, Voli Ave. 13, 43025 Lutsk, Ukraine*

² *Department of Solid-State Physics and Informational-Measurement Technologies, Lesya Ukrainka Eastern European National University, Voli Ave. 13, 43025 Lutsk, Ukraine*

* *Corresponding author. Tel. +380-32-1234567; e-mail: lyuda0760@ukr.net*

Received December 19, 2017; accepted December 27, 2017; available on-line April 1, 2018

The phase diagram of the $\text{TlGaS}_2\text{-CdS}$ system is of the eutectic type, with the coordinates 1021 K, ~80 mol.% TlGaS_2 / ~20 mol.% CdS. The solid solubility of the components is less than 5 mol.% at 670 K. The optical properties of a single crystal of composition 98 mol.% TlGaS_2 / 2 mol.% CdS, grown by the Bridgman method, were investigated. Absorption measurements were performed in the 100-300 K range with 50 K increments. The bandgap energies for direct (E_{gd}) and indirect (E_{gi}) transitions in $\text{TlGaS}_2\text{:Cd}^{2+}$ were calculated as a function of temperature. They were found to be 2.38 and 2.32 eV at 100 K, and 2.27 and 2.2 eV at 300 K, *i.e.* the bandgap for indirect optical transitions is smaller than the bandgap for direct transitions. The values of the direct and indirect bandgap energies decrease with increasing temperature, whereas the steepness parameter and Urbach energy increase with increasing temperature in the range 100-300 K. The Urbach energy was calculated as 163 meV at 100 K and 239 meV at 300 K.

Phase equilibria / Crystal growth / Differential thermal analysis / X-ray diffraction / Urbach energy / Steepness parameter

Introduction

Low-dimensional layered compounds $\text{TlIn}(\text{Ga})\text{X}_2$ ($X = \text{S}, \text{Se}, \text{Te}$) are of interest due to the significant anisotropy of their properties with respect to the crystallographic directions [1]. The crystal structure consists of alternating two-dimensional layers arranged parallel to the (001) plane [2]. The interlayer interaction is of Van der Waals type. Most crystals of this group exhibit both semiconductor and ferroelectric properties and are prone to polytypism. Formation of mixtures of polytypes is also common. TlGaS_2 manifests anisotropy of the electron states near the absorption band edge and is known to crystallize with a number of internal defects that strongly influence the emission and photovoltaic properties. Because TlGaS_2 has high photosensitivity in the visible, infrared and X-ray ranges, these properties make the compound useful for applications in photosensitive devices [3,4].

Given its interesting properties, a great deal of attention has been paid to the study of the structural, electrical and photoelectric properties of TlGaS_2 . Photoconductivity measurements have shown that there is a continuous distribution of traps in the energy gap [5]. Optical absorption measurements have revealed that the undoped compound TlGaS_2 has

direct and indirect energy gaps. But the literature reports disparity in the values of the indirect and direct optical bandgaps. The optical energy of the indirect transitions has been reported as 2.46, 2.38, 2.53, and 2.45 eV, the direct bandgap at room temperature as 2.54, 2.53, 2.58, and 2.63 eV [6-9].

Control of the physical parameters of the ternary compounds may be achieved by partial replacement of the Group III-a ions by ions of other metals. It is known that doping of TlGaS_2 leads to certain changes in the physical properties [10-16].

Here we present the phase equilibria in the $\text{TlGaS}_2\text{-CdS}$ system and the growth and properties of a $\text{TlGaS}_2\text{:Cd}^{2+}$ crystal of the solid solution range (the content of CdS is 2.0 mol.%). The nature of the optical transitions in the region of the fundamental absorption edge, the energy spectrum, the local states in the bandgap, and the possibility of application in semiconductor electronics were determined.

TlGaS_2 is formed at the equimolar ratio of the components in the $\text{Tl}_2\text{S-Ga}_2\text{S}_3$ system and melts congruently at 1165 K [17,18]. Its most stable modifications are the monoclinic (space group $C2/c$, $a = 1.0299$, $b = 1.0284$, $c = 1.5175$ nm, $\beta = 99.7457^\circ$) and the tetragonal ones (S.G. $I4/mcm$, $a = 0.7290$, $c = 2.9900$ nm) [19,20].

The only compound in the Cd-S system, CdS melts congruently and has a narrow homogeneity region [21]. Depending on the formation method, cadmium sulfide crystallizes in the wurtzite (S.G. $P6_3mc$, $a = 0.4137$, $c = 0.6716$ nm) or the sphalerite structure (S.G. $F-43m$, $a = 0.5832$ nm) [22,23], the latter being more likely for thin film deposition.

Experimental

The phase equilibria in the TlGaS₂-CdS system were investigated on 14 alloys that were synthesized from high-purity thallium, cadmium, gallium and sulfur (at least 99.99 wt.% of the main component). Appropriate amounts of the elements were melted in quartz ampoules evacuated to a residual pressure of $1.33 \cdot 10^{-2}$ Pa. The synthesis was performed in a shaft-type furnace. The ampoules were heated to 720 K at the rate of 30 K/h, kept for a day (for complete bonding of elementary sulfur), then heated to 1350 K at 20 K/h. The melts were held at the maximum temperature for 5 h, and then cooled to 670 K at the rate of 10-20 K/h. Homogenizing annealing of the samples was performed at 670 K for 240 h. Finally, the ampoules with the alloys were quenched into cold water.

The alloys were investigated by differential thermal analysis (DTA) and X-ray diffraction (XRD). DTA was performed at a Paulik-Paulik-Erdey derivatograph, using a combined Pt/Pt-Rh thermocouple. The furnace was heated at the rate of 10 K/min and cooled in the inertial mode. X-ray powder patterns were recorded on a DRON-4-13 diffractometer with CuK_α radiation, in the 2θ range 10-80°, with a scan step of 0.05° and 5 s exposure at each point.

The presence of an α -solid solution allows the growth of crystals to study the effect of small admixtures of CdS on the properties of the ternary compound. The crystal growth was performed by the horizontal variation of the Bridgman method of oriented crystallization of the melt. The conditions for the growth of the TlGaS₂:Cd²⁺ crystal (2.0 mol.% CdS) were selected by taking into account literature data on the phase diagram Tl₂S-Ga₂S₃ and the growth of TlGaS₂ single crystals [24,25], and the DTA cooling curves of the samples, to determine the overcooling temperature.

The synthesis of the batch alloy and the crystal growth were combined in one evacuated graphitized quartz container. The growth container with conical bottom was placed at an angle of 10° in a horizontal two-zone electric furnace with independent temperature control. The temperature gradient at the solid-melt interface was 20 K/cm. The maximum temperature in the hot zone was 1150 K. The growth rate was varied in the range 0.1-0.2 mm/h by moving the heating element along the fixed container. A 10 g batch, composed of high-purity elements (at least

99.99 wt.%), was placed in the quartz container, which was evacuated and soldered. The polycrystalline alloy was pre-synthesized according to the above procedure without annealing. The ampoule was placed into the hot zone of the furnace, where the sample melted and was kept for 4-5 h. Then the ampoule with the melt was shifted into the growth zone at the rate of 10 mm/day. After complete crystallization of the melt, annealing for 100 h was performed. Then both zones of the furnace were cooled to room temperature at the rate of 20-30 K/h. A uniform dark-orange single crystal of 30 mm length and 9 mm diameter was obtained.

Results and discussion

The phase diagram of the TlGaS₂-CdS system is presented in Fig. 1. It is of the eutectic type with limited solid solubility of the components (Type V of the Roozeboom classification). The liquidus consists of the curves of crystallization of the solid solution ranges of TlGaS₂ (α) and CdS (β). The solidus is the horizontal line of the invariant eutectic process $L \Leftrightarrow \alpha + \beta$ at 1021 K and the crystallization of the boundary solid solution above this temperature. The coordinates of the eutectic point determined by the Tamman triangle are ~80 mol.% TlGaS₂ and ~20 mol.% CdS.

Typical diffraction patterns of the alloys of the system are presented in Fig. 2. The intermediate alloys feature combinations of two sets of diffracted reflections, the intensity ratio correlating well with the content of the system components. The solid solubility in CdS at 670 K is less than 5 mol.% TlGaS₂. The boundary of the solid solution range of TlGaS₂ lies between 2.5 and 5 mol.% CdS.

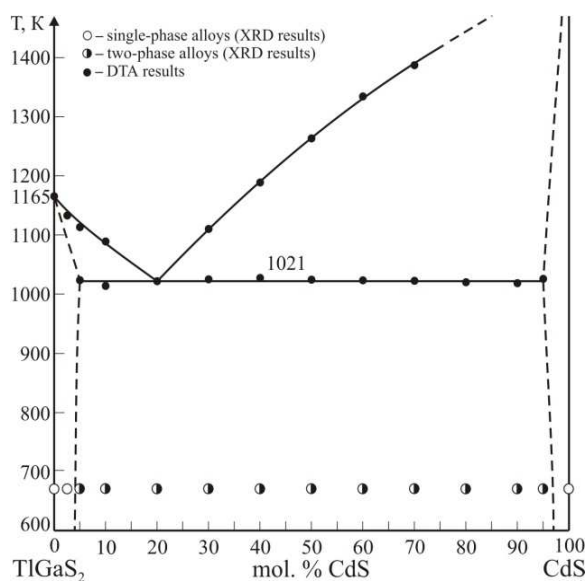


Fig. 1 Phase diagram of the TlGaS₂-CdS system.

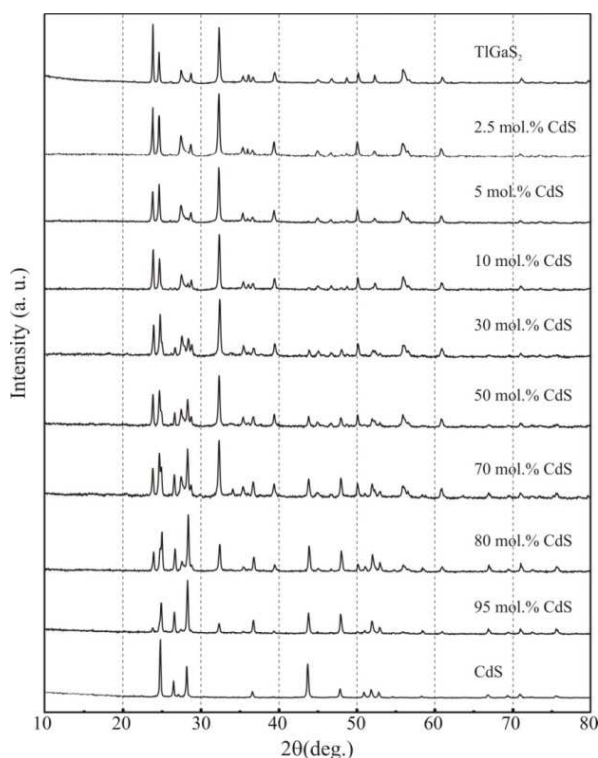


Fig. 2 XRD patterns of alloys in the TlGaS₂–CdS system.

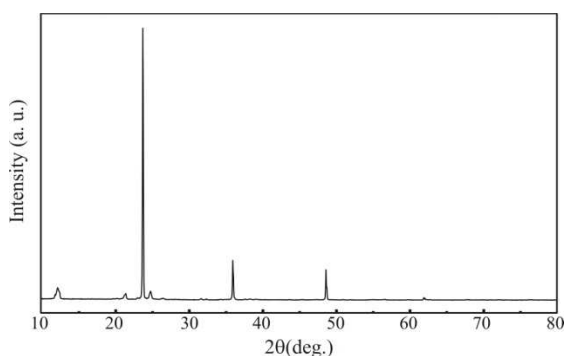


Fig. 3 Diffraction pattern of the TlGaS₂:Cd²⁺ single crystal on the reflection of a naturally cleaved surface (001).

The identity of the crystal structure (S.G. *C2/c*) of the grown crystal with that of the original TlGaS₂ was confirmed by X-ray powder diffraction. The diffraction pattern of the single-crystalline sample on the reflection of a naturally cleaved surface (001) is presented in Fig. 3.

For the optical absorption spectra thin-plate samples of the TlGaS₂:Cd²⁺ single crystal were cleaved from the single-crystalline ingot. The incident light was parallel to the crystallographic axis *c*, *i.e.* perpendicular to the layers. The investigation of the optical transmission spectra was performed using a nitrogen cryostat with an available temperature range of 77–380 K (± 0.2 K accuracy). An MDR-206

monochromator (wavelength accuracy ± 0.5 nm) was used as spectrograph. The absorption measurements were performed in the temperature range 100–300 K.

The absorption coefficients were calculated from the experimental data using the following formula [26]:

$$T = (1 - R)^2 \exp(-A) = (1 - R)^2 \exp(-\alpha d), \quad (1)$$

where *R* is the reflectivity, α the optical absorption coefficient (cm⁻¹), and *d* the sample thickness. Optical absorption coefficients were determined for all temperatures using the value of *R* at room temperature, assuming that the change in temperature from 10 to 320 K has little effect on *R* [27]. Multiple reflections were dealt with by placing the sample at a small angle with respect to the incident beam. The fundamental absorption edge in most semiconductors follows the exponential law. It was observed that the absorption coefficient of the semiconductor above the exponential tail adheres to the equation:

$$\alpha h\nu = B(h\nu - E_g)^n, \quad (2)$$

where α is the absorption coefficient, and *B* is a constant; the factor *n* depends on the nature of the electron transition responsible for absorption and takes the values $n = 1/2$ for direct allowed transitions (high-energy part of the spectra), $n = 3/2$ for forbidden direct transitions, $n = 2$ for indirect allowed transitions (low-energy part of the spectra), and $n = 3$ for forbidden indirect transitions [28].

The exponentially increasing absorption edge in a number of insulators, including ionic crystals, semiconductors and organic crystals, follows an empirical expression [29]:

$$\alpha = \alpha_0 \exp\left[\frac{\sigma(h\nu - E_0)}{k_B T}\right] \quad (3)$$

where α_0 and E_0 are characteristic parameters of the material, σ is the steepness parameter, and k_B is Boltzmann's constant. The temperature dependence of the steepness parameter σ , which characterizes the slope near the absorption edge, is empirically expressed as [30]:

$$\sigma = \sigma_0 \left(\frac{2k_B T}{h\nu_0} \right) \tanh\left(\frac{h\nu_0}{2k_B T} \right), \quad (4)$$

where σ_0 is a temperature-independent, material-specific parameter. Some researchers consider that $h\nu_0$ corresponds to the energy of phonons associated with the Urbach tail. The absorption coefficients obtained for the 1s-exciton by taking into account only the quadratic term of the exciton-phonon interaction operator are very similar to the coefficients expressed by Eq. 3. The parameter $\sigma/k_B T$ for the interaction between excitons and longitudinal optical phonons coincides with Eq. 4 with a constant multiplier [31].

The temperature dependence of the bandgap energy is often empirically expressed as [32]:

$$E_g(T) = E_g(0) - \delta \frac{T^2}{T + \beta}, \quad (5)$$

where $E_g(T)$ is the bandgap energy, $E_g(0)$ is the bandgap energy at 0 K, and δ and β are material-specific constants. The constant β is approximately equal to the Debye temperature Θ_D . The thermal change in the bandgap width was determined as follows:

$$\frac{dE_g}{dT} = \left(\frac{dE_g}{dT} \right)_{l-ex} + \left(\frac{dE_g}{dT} \right)_{e-p}, \quad (6)$$

where the first and second members represent the expansion of the lattice and the electron-phonon interaction, respectively.

The spectral dependence of the absorption coefficient in the temperature range 100-300 K was investigated to study the energy gap and possible interband transitions in the TlGaS₂:Cd²⁺ crystal. Typical plots obtained at 100, 150, 200, 250, and 300 K are presented in Fig. 4. The absorption coefficients range from 58 to 882 cm⁻¹.

To estimate the bandgap energy for indirect (E_{gi}) and direct (E_{gd}) allowed transitions, the lines $(\alpha h\nu)^{1/2} = f(h\nu)$ and $(\alpha h\nu)^2 = f(h\nu)$ were extrapolated to $(\alpha h\nu)^{1/2} = 0$ and $(\alpha h\nu)^2 = 0$ (Figs. 5,6) [33-35].

The temperature dependence of the bandgap energy for indirect and direct transitions in the temperature range 100 to 300 K is shown in Fig. 7. The bandgap energy for the direct permitted transitions E_{gd} is 2.27 eV at 300 K, that for the indirect transitions (E_{gi}) is 2.2 eV. The values of the indirect and direct energy gaps for the TlGaS₂:Cd²⁺ crystal at different temperatures are listed in Table 1.

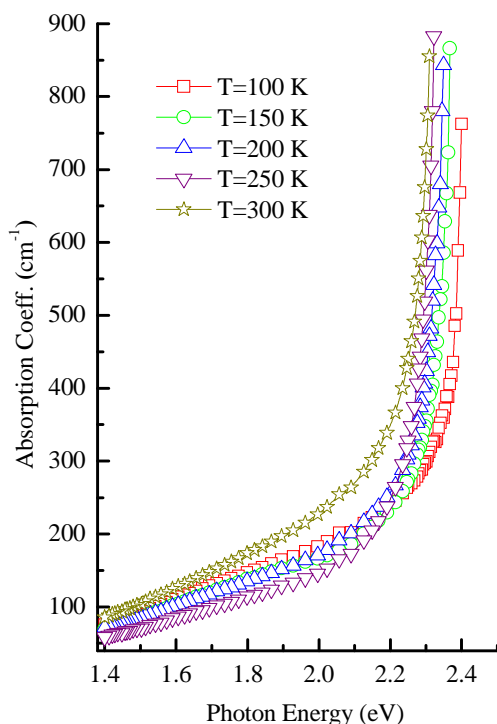


Fig. 4 Spectral dependence of the absorption coefficient of the TlGaS₂:Cd²⁺ crystal.

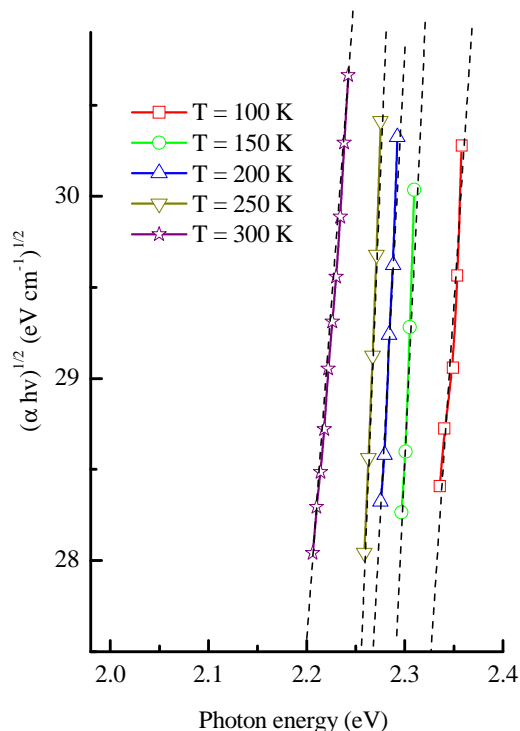


Fig. 5 Spectral dependence of $(\alpha h\nu)^{1/2}$ for the TlGaS₂:Cd²⁺ crystal.

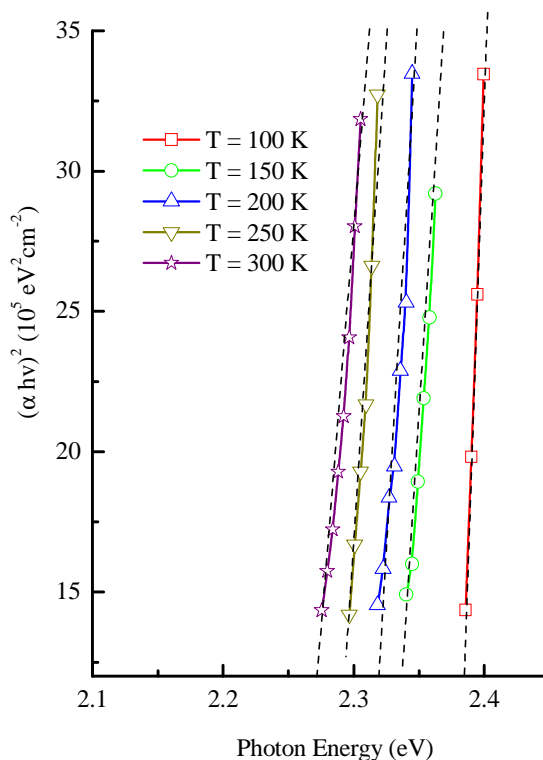
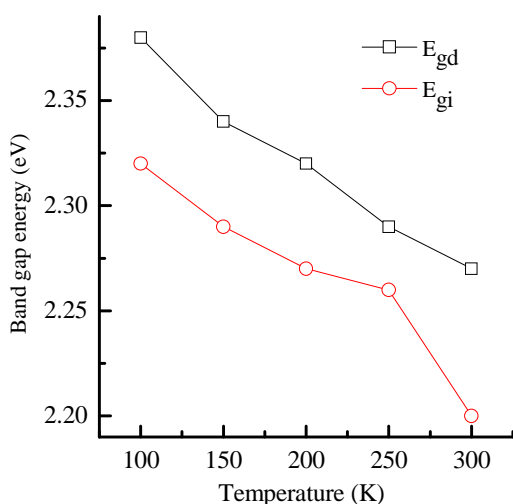


Fig. 6 Spectral dependence of $(\alpha h\nu)^2$ for the TlGaS₂:Cd²⁺ crystal

Table 1 Direct (E_{gd}) and indirect (E_{gi}) bandgap energy, Urbach energy and steepness parameter for the TlGaS₂:Cd²⁺ crystal.

Sample	Sample temperature, K	E_{gd} , eV	E_{gi} , eV	Urbach energy, meV	Steepness parameter
TlGaS ₂ :Cd ²⁺	100	2.38	2.32	163	0.053
	150	2.34	2.29	178	0.073
	200	2.32	2.27	195	0.088
	250	2.29	2.26	218	0.099
	300	2.27	2.2	239	0.108

**Fig. 7** Temperature dependence of the bandgap energy for direct (E_{gd}) and indirect (E_{gi}) permitted transitions.

Urbach's tails were observed at all temperatures (100-300 K). Typical Urbach's tails for various temperatures are shown in Fig. 8. It was found that the extrapolations of the Urbach's tails converge at the point $(E_0, \alpha_0) = 2.8$ eV, 2000 cm⁻¹. These results show that the absorption spectra follow Urbach's rule.

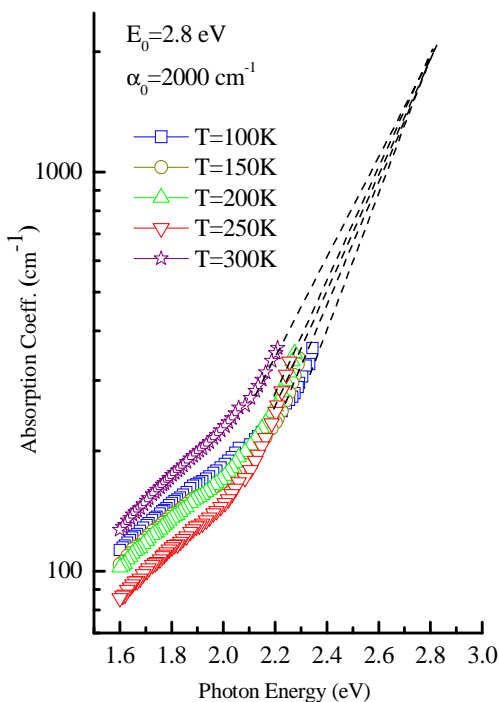
The bandgap for indirect optical transitions in TlGaS₂:Cd²⁺ is narrower than that for direct optical transitions. In either case, the bandgap energy decreases with increasing temperature. These results are consistent with previous studies [36-38]. The direct and indirect temperature coefficients for TlGaS₂:Cd²⁺, calculated from Eq. 6, are $dE_{gd}/dT = -5.5 \cdot 10^{-4}$ eV/K and $dE_{gi}/dT = -6 \cdot 10^{-4}$ eV/K, which agrees well with the results of [30-32]. These values are typical for crystals with layered structure. The temperature coefficient of the bandgap energy depends both on the expansion of the lattice and the electron-phonon interaction. The sign of the temperature coefficient as expressed in Eq. 6 does not depend on the sign of the first or the second term, but the total temperature coefficient depends on the nature of the system, especially on the electronic wave functions. It was found that the temperature coefficients of the bandgap energy of TlGaS₂:Cd²⁺ have negative signs, which suggests that the

contribution of the electron-phonon interaction is greater than that of the lattice expansion [33,34].

The Urbach energy ($k_B T/\sigma$), which corresponds to the inverse of the slope of the Urbach tails, and the steepness parameter (σ) for the TlGaS₂:Cd²⁺ samples are plotted as a function of temperature in Fig. 9 (the solid line is the best fit to the experimental points).

To obtain an estimate of the values of the phonon energies associated with the Urbach tails, the experimental data $\sigma(T)$ were treated by Eq. 4 with σ_0 and $h\nu_0$ as adjustable parameters. Both parameters, the steepness and Urbach energy, increase with the sample temperature in the range 100-300 K (Table 1). These results are consistent with data reported in the literature [28,35-38].

The lower values of the Urbach energy at lower temperatures are explained by the recharging of defective centers when the temperature is lowered. This leads to the neutralization of part of the charged defects and the reduction of their influence on the random modulation of the electric field in the sample.

**Fig. 8** Spectral dependence of the absorption coefficient of TlGaS₂:Cd²⁺ at different temperatures.

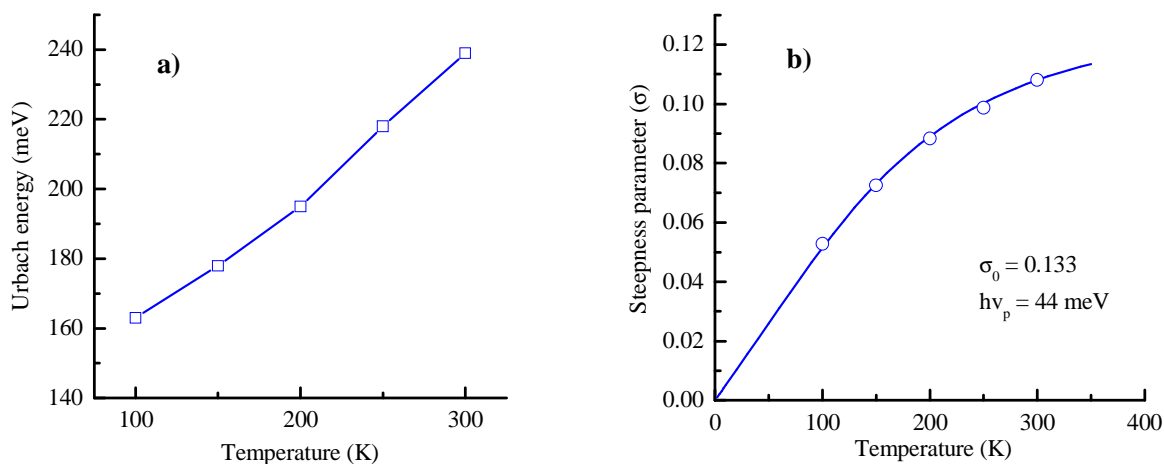


Fig. 9 Dependence of the Urbach energy (a) and the steepness parameter (b) on temperature.

Conclusions

The phase diagram of the TiGaS₂-CdS system was investigated. It is of the eutectic type with limited solid solubility of the components (less than 5 mol.% in either direction). The coordinates of the eutectic point are 20 mol.% CdS and 1021 K.

A single crystal of TiGaS₂ doped with 2.0 mol.% CdS was grown by the horizontal version of the Bridgman-Stockbarger method, using the experimental conditions determined from the constructed phase diagram, and its optical properties were studied. The bandgap energies for direct and indirect permitted transitions were estimated from the spectral distribution of the absorption coefficient in the temperature range 100-300 K. The bandgaps for the direct and indirect transitions were calculated as 2.38 and 2.32 eV at 100 K and 2.27 and 2.2 eV at 300 K. It was established that doping with Cd²⁺ leads to a slight decrease of both bandgap energies compared to the original TiGaS₂ crystal. The temperature coefficients of the bandgap energy of TiGaS₂:Cd²⁺ have negative signs, which suggests that the contribution of the electron-phonon interaction is greater than that of the lattice expansion. It follows that the energy of phonons $h\nu_{ph}$, which is higher than the highest optical mode of the TiGaS₂ crystals, is associated with structural and compositional disorder.

The Urbach energy decreased with decreasing temperature (from 239 meV at 300 K to 163 meV at 100 K). We consider that this is due to the recharging of defective centers at lower temperature, thus neutralizing some of the charged defects and decreasing their effect on the random modulation of the electric field.

References

- [1] F.V. Perez, R. Cadenas, C. Pover, J. Gonzales, C.J. Chervin, *J. Appl. Phys.* 101 (2007) 063534.
- [2] M.S. Jin, H.J. Song, *Curr. Appl. Phys.* 3 (2003) 409.
- [3] G.E. Delgado, A.J. Mora, F.V. Perez, J. Gonzalez, *Phys. B* 391 (2007) 385.
- [4] A.F. Qasrawi, N.M. Gasanly, *Phys. Status Solidi A* 202 (2005) 2501.
- [5] I.M. Ashraf, *J. Phys. Chem. B* 108 (2004) 10765.
- [6] A.E. Bakhyshev, A.A. Lebedev, Z.D. Khalafov, M.A. Yakobsan, *Sov. Phys. Semicond.* 12 (1978) 320.
- [7] M.P. Haniyas, A.N. Anagnostopoulos, K. Kambas, J. Spyridelis, *Mater. Res. Bull.* 27 (1992) 25.
- [8] B. Gurbulak, *Phys. Status Solidi A* 184 (2001) 349.
- [9] N.M. Gasanly, *J. Kor. Phys. Soc.* 57 (2010) 164.
- [10] A.U. Malsagov, B.S. Kulbuzhiev, B.M. Khamkhoyev, *Izv. Akad. Nauk SSSR, Neorg. Mater.* 25 (1989) 216.
- [11] M. Açikgöz, *Turk. J. Phys.* 32 (2008) 145.
- [12] S.N. Mustafaeva, *Neorg. Mater.* 45 (2009) 659.
- [13] O. Karabulut, K. Yilmaz, B. Boz, *Cryst. Res. Technol.* 46 (2011) 79.
- [14] S.N. Mustafaeva, S.G. Jafarova, E.M. Kerimova, S.M. Asadov, R.G. Mamedov, *Proc. Int. Conf. "Fundamental and Applied Problems of Physics"*, Tashkent, 2017, pp. 5-8.
- [15] S.N. Mustafaeva, *Zh. Radioelektron.* 8 (2008) 1.
- [16] S.N. Mustafaeva, M.M. Asadov, S.B. Kyazimov, N.Z. Gasanov, *Neorg. Mater.* 48 (2012) 984.
- [17] Y. Guittard, M. Palazzi, C. Ecrepont, *Mater. Res. Bull.* 26 (1991) 137.

- [18] O. Tsisar, L. Piskach, A. Fedorchuk, O. Parasyuk, L. Marushko, B. Kotur, *Proc. Shevchenko Sci. Soc. Chem. Sci.* XLVIII (2017) 75.
- [19] F.V. Perez, J. Gonzalez, A.J. Mora, G.E. Delgado, *Ciencia* 16 (2008) 55.
- [20] H. Hahn, B. Wellman, *Naturwissenschaften* 54 (1967) 42.
- [21] R.C. Sharma, Y.A. Chang, *J. Phase Equilib.* 17 (1996) 425.
- [22] M. Ikeda, H. Wada, T. Wada, T. Hirao, *J. Cryst. Growth* 135 (1994) 476.
- [23] C. Bourouis, A. Meddour, *J. Magn. Magn. Mater.* 324 (2012) 1040.
- [24] K.T. Vilke, *Growth of Crystals*, Nedra, Leningrad, 1977 (in Russian).
- [25] Yu.M. Tairov, V.F. Tsvetkov, *Technology of Semiconductor and Dielectric Materials*, Vysshaya Shkola, Moscow, 1990 (in Russian).
- [26] T.S. Moss, *Optical Processes in Semiconductors*, Butterworths, London, 1959.
- [27] M. Haniyas, A. Anagnostopoulos, K. Kambas, J. Spyridelis, *Phys. B* 160 (1989) 154.
- [28] J.I. Pankove, *Optical Process in Semiconductors*, Dove, New York, 1975.
- [29] F. Urbach, *Phys. Rev.* 92 (1953) 1324.
- [30] H.W. Martienssen, *J. Phys. Chem. Solids* 2, (1957) 257.
- [31] K.R. Allakhverdiev, M.A. Aldzhonov, T.G. Mamedov, E.Yu. Salaev, *Solid State Commun.* 58 (1986) 295.
- [32] Y.P. Varshni, *Physica* 34 (1967) 149.
- [33] R.A. Aliev, K.R. Allakhverdiev, A.I. Baranov, N.R. Ivanov, R.M. Sardarly, *Fiz. Tverd. Tela* 27 (1985) 2836.
- [34] N.S. Yuksek, N.M. Gasanly, H. Ozkan, *Semicond. Sci. Technol.* 18 (2003) 834.
- [35] A.F. Qasrawi, N.M. Gasanly, *Semicond. Sci. Technol.* 19 (2004) 505.
- [36] B. Gurbulak, *Appl. Phys. A* 68 (1999) 353.
- [37] G.L. Myronchuk, G.E. Davydyuk, O.V. Parasyuk, O.Y. Khyzhun, R.A. Andrievski, A.O. Fedorchuk, S.P. Danylchuk, L.V. Piskach, M.Yu. Mozolyuk, *J. Mater. Sci: Mater. Electron.* 24 (2013) 3555.
- [38] G. Makhnovets, G. Myronchuk, L. Piskach, B. Vidrynskyi, A. Kevshyn, *Ukr. Zh. Fiz. Opt.* 19 (2018) 49.